Applied Energy 147 (2015) 510–522

Contents lists available at ScienceDirect

Applied Energy

journal homepage: www.elsevier.com/locate/apenergy

Characterising the spatial and temporal variability of the tidal-stream energy resource over the northwest European shelf seas

Peter E. Robins *, Simon P. Neill, Matt J. Lewis, Sophie L. Ward

School of Ocean Sciences, Bangor University, LL59 5AB, UK

HIGHLIGHTS

- Model characterisation of the European tidal-stream energy resource.
- The mean spring tide may underestimate the resource by up to 25%.
- Tidal-stream variability at lunar to tidal scales affects power generation by 15%.

ARTICLE INFO

Article history:
Received 13 January 2015
Received in revised form 5 March 2015
Accepted 6 March 2015
Available online 22 March 2015

Keywords:
Tidal-stream resource
Tidal energy
ROMS
Tidal model
Northwest European shelf

ABSTRACT

As devices move from full-scale prototype to commercial installations, it is important that developers have detailed knowledge of the tidal energy resource. Therefore, the spatial distribution of the tidal currents over the northwest European shelf seas has been examined to improve understanding of the tidal-stream energy resource. Using a three-dimensional hydrodynamic model (ROMS) at ~1 km spatial resolution, and applying device characteristics of the Seagen-S turbine, we show that the ratio of the amplitudes of the M_2 and S_2 tidal currents can lead to significant variability in annual practical power generation – variability that is not accounted for when considering only the mean peak spring tidal velocities, as is generally the case in resource feasibility studies. In addition, we show that diurnal inequalities (governed by K_1 and O_1 tidal constituents) and tidal asymmetries (governed by the relationship between M_2 and its compound tide M_4) over the northwest European shelf seas can further affect power generation at potential high-energy sites. Based on these variabilities, the spatial distribution of the tidal-stream 'capacity factor' has been calculated. We find that mean peak spring tidal velocities can under-estimate the resource by up to 25%, and that annual practical power generation can vary by ~15% for regions experiencing similar mean peak spring tidal velocities, due to the influence of other tidal constituents. Therefore, even preliminary resource assessments should be based on annual average power density, rather than peak spring tidal velocity.

1. Introduction

The tidal-stream renewable energy industry – where the kinetic energy inherent in the oceans is converted into low carbon electricity – is at a crucial stage of development, where single-device tidal-stream energy converters (TECs) have been installed and grid-connected at high-energy sites (e.g., www.marineturbines.com; www.openhydro.com). The next stage – the construction of offshore tidal energy farms, or TEC arrays – has been granted consent at several sites around the world (e.g., www.fundayforce.ca; www.emec.org.uk; www.thecrownestate.co.uk). Initial site selection for these locations has generally been informed by relatively superficial resource assessment modelling products (e.g., BERR Atlas of UK Marine Renewables; [1], with particular emphasis on the magnitude of the peak spring tidal currents. However, there are a number of tidal resource assessments in which mean peak spring tidal velocities are not used, for example, Ramos et al. [2]. A number of factors should be considered within any resource assessment, such as power generation, temporal variability within the resource, site conditions (e.g., distance to grid connection), as well as practical and socioeconomic constraints relating to grid infrastructure [3], governmental strategy on low carbon energy (e.g., the 'Renewables Obligation' for the UK; www.ofgem.gov.uk), and potential environmental impacts (e.g. [4–7].

Whilst the most attractive sites around the world suitable for tidal-stream development are well known, and are characterised

* Corresponding author.
E-mail address: p.robins@bangor.ac.uk (P.E. Robins).

http://dx.doi.org/10.1016/j.apenergy.2015.03.045
0306-2619/

by very strong tidal flow (e.g. [8,9]), a more detailed analysis of the resource is required in order to reduce investor risk and help developers choose the best locations for their technologies, as well as to advise governments on resource optimisation according to their strategic energy plan. We propose that particular emphasis has been placed on tidal current magnitude for site selection and not on its temporal variability, and the resultant net power. For example, a site which has a lower peak tidal current than another site may actually have a greater net resource, because the time series velocities are more consistent, more symmetrical between the flood and ebb phases of the tidal cycle, or less influenced by atmospheric processes. Indeed, both Hashemi et al. [10] and Lewis et al. [11] have demonstrated the impacts of waves and wave-tide misalignment on the tidal currents in the Irish Sea – the waves altering the predicted tidal currents by up to ±10%. Lewis et al. [12] have highlighted the implications of tidal current misalignment (for fixed-orientation, horizontal-axis turbines), as well as the limitations of the resource due to water depth of deployment. Neill et al. [13] show the role of tidal asymmetry for a semi-constricted channel in the Orkney archipelago.

Several tidal-stream resource assessments (e.g., [14,15]) have studied tidal phasing and optimisation methods. Neill et al. [15] introduce the issue of tidal phasing in relation to resource optimisation over the European shelf, to generate 'firm tidal power', or a continuous source of low-carbon electricity to the grid. Power generation from regions of greatest tidal-stream resource (e.g., Orkney, the Channel Islands, and the eastern Irish Sea) are approximately in-phase with one another and, hence, aggregated power generation at these sites will be characterised by modulation at the quarter-diurnal period (i.e., sub-optimal power will be generated around each period of slack water, approximately four times per day). However, little research has been conducted on the temporal variability of the tidal-stream resource, and how this varies spatially, which is essential when considering the ultimate goal of firm power generation.

Here, we investigate the spatial and temporal variability of the magnitude of the tidal currents and potential power production across the northwest European shelf seas, with the aim of improving our understanding of the net tidal-stream energy resource and optimising energy yield. We have simulated tidal flow over the shelf using the three-dimensional Regional Ocean Modelling System (ROMS), applied at higher spatial resolution (~1 km) than has previously been achieved at this scale (e.g., [10,15]). Although a 3D model has been implemented, results are presented on the basis of depth-averaged velocities. These waters are some of the most energetic in the world in terms of tidal energy dissipation (i.e., dissipating approximately 10% (0.25 TW) of global tidal energy; [9], and this study will therefore add considerable value to the European marine renewable energy industry in terms of resource assessment and potential optimisation strategies, and our methodology could be applied to other regions of the world with an energetic tidal resource.

This paper is structured as follows: Section 2 describes the theory of tidal variability over the northwest European shelf seas; model characteristics and validation are described in Section 3; analysis of the tidal current variability is presented in Section 4, enabling the tidal-stream energy resource to be mapped according to the criteria explained above; our discussions and conclusions (Sections 5 and 6, respectively) are then presented in the final sections.

2. Tidal variability

Tidal currents are driven by oceanic pressure gradients associated with the gravitational attraction between the Earth and the Moon (lunar) and the Sun (solar), and their respective rotations [16,17]. In most locations, the largest tidal constituent is the principal lunar semi-diurnal (M_2), which has a period of approximately 12.42 h – exactly half the time required for the Earth to rotate once relative to the Moon. In the same way, the 'principal solar semi-diurnal' (S_2) tidal constituent, which has approximately half the force of M_2, has a period of 12 h – half a solar day. The propagation of tidal currents in the deep ocean is primarily governed by the linear superposition of M_2 and S_2, which are in-phase every ~14.75 days, producing aggregated tidal currents (springs), and out-of-phase in between, producing minimum tidal currents (neaps). Sub-optimal power generation will occur during neap tides and full power potential is not realised during spring tides at some sites. Here, we describe only tidal currents; in addition, ocean currents may comprise other, non-tidal drivers, such as wind and density gradients, which may contribute to, or reduce, the available power resource.

We considered variability in the tidal currents over the lunar (spring-neap) cycle. Variability in the magnitude of S_2 tidal currents, relative to M_2, occurs due to differences in quadratic friction (with more friction at spring tides), and rotation between the two harmonics, which causes differences in the positions of their respective amphidromic points [18]. Here, lunar variability in tidal currents was quantified according to the following ratio (R):

$$R = 1 - \left(\overline{U}_{S2}/\overline{U}_{M2}\right) \tag{1}$$

where $\overline{U}_{M2}$ and $\overline{U}_{S2}$ denote the amplitudes of the depth-averaged tidal velocity at each model cell. The inverse ratio has been used in Eq. (1) so that higher values signify a large M_2 velocity amplitude relative to S_2, which is desirable for energy exploitation at lunar timescales, given two sites of similar mean spring peak flow.

Beyond the well-known spring-neap tidal cycle that describes the interaction between M_2 and S_2, a number of other harmonic signals exist within the tide that vary spatially. Firstly, we look at the daily modulation of the tide, as two consecutive tides can be significantly different due to the declination of the Moon [16], and are described by the interaction between the diurnal K_1 and O_1 harmonics. The 'tidal form' varies around the globe, arising from local differences in semi-diurnal and diurnal forcing constituents, resulting in tides that range from strongly semi-diurnal to strongly diurnal [19]. Pond and Pickard [19] classifies the Form ratio as:

$$F = \frac{(H_{K1} + H_{O1})}{(H_{M2} + H_{S2})} \tag{2a}$$

where H signifies the amplitudes of tidal elevation; $F > 3$ indicates diurnal tides, whereas $F < 0.25$ indicates semi-diurnal tides. Here, we classify the daily modulation of the tidal currents over the northwest European shelf seas, defined by the tidal current Form ratio (Fu):

$$Fu = \frac{\left(\overline{U}_{K1} + \overline{U}_{O1}\right)}{\left(\overline{U}_{M2} + \overline{U}_{S2}\right)} \tag{2b}$$

which is based on the sum of the depth-averaged tidal current amplitudes of the two principal diurnal constituents to that of the two principal semi-diurnal constituents. If the tide is strongly semi-diurnal, then equal amounts of power will be generated on two consecutive tides. As the diurnal inequality strengthens, in regions where the combined $\overline{U}_{K1}$ and $\overline{U}_{O1}$ diurnal current amplitudes are significant, power generation may become sub-optimal for one of these tides per day, hence, variability in peak power generation per tide per day. The northwest European shelf seas are strongly semi-diurnal, and F is generally less than 0.25; however, small variations in F, and hence Fu, will potentially generate significant variability in the amount of practical power produced. Based on this, we hypothesise that, for sites with similar peak

depth-averaged currents, diurnal inequalities (i.e., higher values of *Fu*) will reduce the available practical power, compared with sites that are strongly semi-diurnal (i.e., lower values of *Fu*).

Finally, we look at tidal asymmetries and, hence, variability in power generation over semi-diurnal timescales. Nonlinear processes such as friction, advection (due to advective inertia forces), and diffusion (due to turbulence) produce significant super-harmonics of M_2 which manifest the tidal currents into a more complex signal comprising overtides – such as M_4 [13]. M_4-generated tidal asymmetries are particularly pronounced over shallow continental shelf regions [20], where tidal energy exploitation will concentrate and, hence, will produce asymmetries in power extraction, reducing the overall energy yield [5]. It is generally the phase relationship between the principal semi-diurnal tidal current (M_2) and its quarter-diurnal first harmonic (M_4) that describes this tidal asymmetry [20], in addition to the M_2:M_4 magnitude ratio.

The phase relationship between the principal semi-diurnal tidal current ($\emptyset_{\overline{UM2}}$) and its quarter-diurnal harmonic ($\emptyset_{\overline{UM4}}$) has been calculated, according to Pingree and Griffith [20], as $2\emptyset_{\overline{UM2}} - \emptyset_{\overline{UM4}}$. This relationship represents M_4-generated tidal asymmetry, where all theoretical combinations of $2\emptyset_{\overline{UM2}} - \emptyset_{\overline{UM4}}$ lie within the range −360° to +720°. Therefore, this relationship was normalised, spatially, to produce a relative phase relationship (within the range 0–360°), by subtracting the minimum theoretical phase relationship, relative to the local $\emptyset_{\overline{UM2}}$, i.e.:

$$A = \sin\left[\left[2\emptyset_{\overline{UM2}(i,j)} - \emptyset_{\overline{UM4}(i,j)}\right] - \min\left[2\emptyset_{\overline{UM2}(i,j)} - \emptyset_{\overline{U}(k)}\right]_{k=0}^{k=360^\circ}\right] \quad (3)$$

where i and j denote the eastwards and northwards model cell position, respectively. In Eq. (3), the sine of the relative phase relationship has been equated to a metric for tidal asymmetry (A), which denotes the (normalised) mean depth-averaged flood velocity divided by the ebb velocity [13]. In the case where the flood and ebb currents are equal, the relative phase relationship is 90° and A = zero, and so power generated on the flood and ebb phases of the tide is equal. Yet when the relative phase relationship is 0°, or 180°, A = ±1 and maximum asymmetry occurs; i.e., stronger velocities during the flooding tide than during the ebbing tide, or vice-versa. Consequently, provided the tidal current amplitude of M_4 is significant, relative to that of M_2, maximum power generation may occur once per tidal cycle, rather than twice, and the overall power production is reduced, compared with the symmetrical case, even though peak velocity is higher. Therefore, we also hypothesise that the overall energy yield is reduced for large M_4 tidal amplitudes that generate tidal asymmetry.

The above processes described by the additional tidal harmonics O_1, K_1, and M_4 are not routinely incorporated into tidal-stream resource maps or optimal resource exploitation studies. However, Polagye and Thomson [21] address some of these processes for a case study in the Puget Sound, USA; specifically, they calculate several metrics to characterise the resource at sites in Admiralty Inlet, including a power metric based on the mean kinetic power asymmetry between the flood and ebb currents. As we propose, Polagye and Thomson [21] also voice caution in using mean velocity as a metric for tidal resource assessments. Following Polagye and Thomson [21], we suggest improvements to the way in which the tidal-stream resource map is characterised, based on magnitude and temporal variability in power production, rather than traditional resource maps based on mean spring peak velocities. Polagye and Thomson [21] considered harmonic variability in the tidal currents collectively, when calculating net power densities, whereas our approach investigates the variability of the principal tidal constituents discretely, in order to improve the overall resource characterisation.

3. Tidal model

Three-dimensional tidal currents were simulated over the northwest European shelf seas using ROMS (Regional Ocean Modelling system) – a free surface, terrain-following, primitive equations ocean model. The hydrodynamics of ROMS are based on the Reynolds-averaged Navier-Stokes equations, with hydrostatic and Boussinesq assumptions [22,23]. A detailed description of the numerical algorithms of ROMS were presented by Shchepetkin and McWilliams [22].

3.1. Data input

Our domain extended from 14° W to 11° E, and 42° N to 62° N (Fig. 1a). The domain was discretised with a horizontal curvilinear grid, applying a variable longitudinal resolution of 1/60° (0.87–1.38 km), and a latitudinal resolution of 1/100° (~1.11 km). The bathymetric grid is based on GEBCO global data (www.gebco.net) at 1/120° spatial resolution. The vertical grid consists of 10 layers distributed according to the ROMS terrain-following coordinate system. Therefore, the model domain comprises 30 million discrete computational cells, approximately 40% of which are land cells. The open boundaries of the model were forced by tidal elevation (Chapman boundary condition) and tidal velocities (Flather boundary condition), generated by 10 tidal constituents (M_2, S_2, N_2, K_2, K_1, O_1, P_1, Q_1, M_f, and M_m) obtained from TPX07 global tide data with 1/4° resolution [24]; volkov.oce.orst.edu/tides). The physical compilation specifications for our application were: quadratic bottom friction (0.003 non-dimensional drag coefficient), horizontal and vertical mixing of momentum, the generic length scale turbulent closure model tuned to $k-\varepsilon$ (p = 3, m = 1.5, and n = 1; *see* [25]. Analogous examples of ROMS applications include: Haidvogel et al. [26], Neill et al. [15], Hashemi and Neill [27], and Lewis et al. [12].

3.2. Implementation and validation

Robust estimates of the long-term power generation potential of a site require an observation/simulation period of at least 30 days [21]. Our simulation period was 32 days, generating output every 0.5 h after an initial 2-day model spin-up. Hence, we use 30 days of tidal simulation for our tidal analysis, which is sufficient for analysis of the following principal constituents: M_2, S_2, K_1, O_1, and M_4. Tidal analysis was performed on simulated elevations and depth-averaged velocities (i.e., approximately 2.35 million separate analyses) over the 30-day period, producing calculations of tidal current amplitudes and phases. Analyses were performed using T_TIDE [28].

Our simulated elevations were validated at 20 coastal locations (*see* Fig. 1b) against tide gauge data available from the UK National Oceanography Centre (www.ntslf.org). The M_2 and S_2 semi-diurnal tides are the primary tidal constituents across the shelf, and therefore for validation we analysed modelled M_2 and S_2 elevations from the cell nearest to each tide gauge. Our simulation produced M_2 and S_2 root mean squared errors (RMSE) of 15 cm and 5 cm in amplitude, and 12° and 10° in phase, respectively (Fig. 1b), which are comparable to other modelling studies of the shelf [10,29,30]. To validate our simulated tidal current speeds, comparisons were made between the simulated depth-averaged currents and data from 15 tidal current meters [31–33]; Fig. 1b). Again, the analysed currents from the model cell nearest to each current meter were compared to the data, producing M_2 and S_2 RMSE of 0.046 m s^{-1} and 0.016 m s^{-1} in amplitude, and 12° and 12° in phase, respectively (Fig. 1b). Again, these errors are comparable to other modelling studies of the shelf (Neill et al. 2010). Also shown in Fig. 1b are the calculated scatter indices (SI), i.e., RMSE normalised

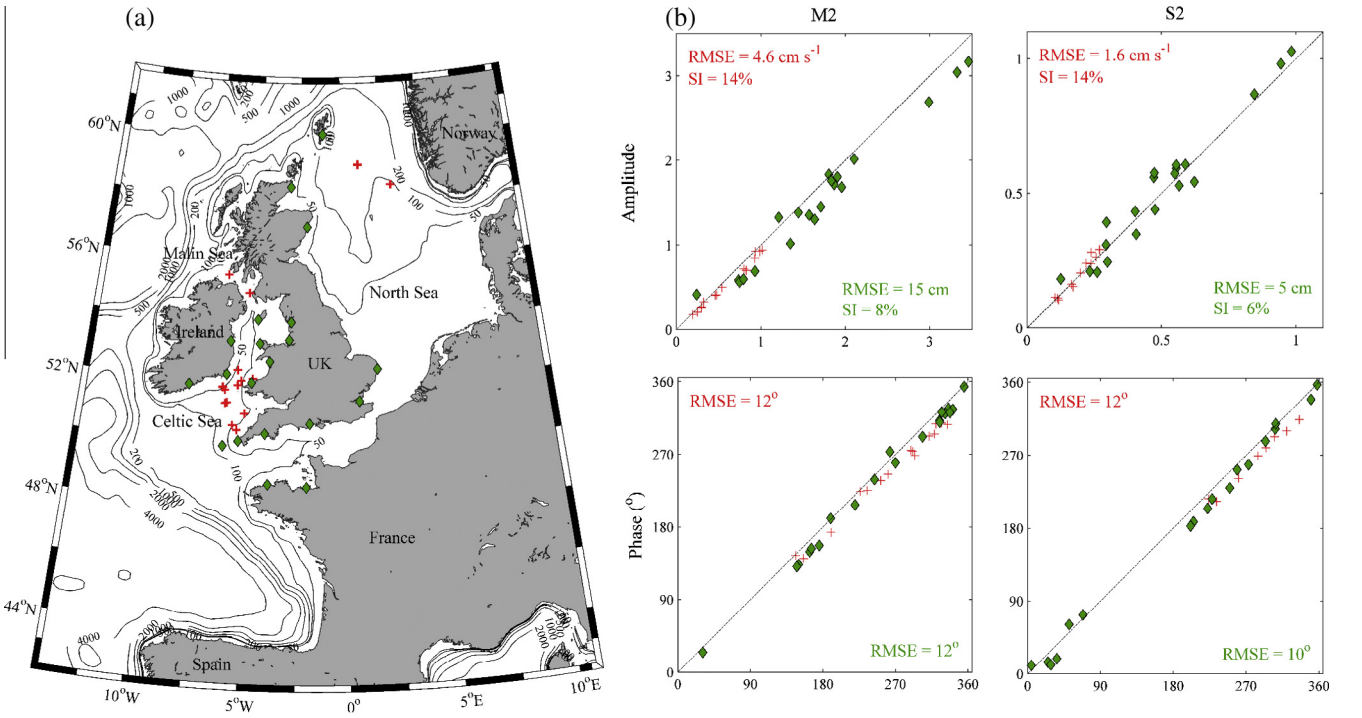

Fig. 1. (a) Our ROMS domain of the northwest European shelf seas, showing bathymetry (in meters, relative to mean sea level) and model validation points (tide gauge stations = diamonds, velocity data = crosses). (b) Model-data comparisons and statistics (root mean squared error (RMSE) and scatter index (SI)) for M_2 and S_2 amplitude and phase of elevations and depth-averaged velocities, respectively.

by the mean of the observations, and given as percentages ($\leqslant$8% SI for elevations and $\leqslant$14% SI for tidal currents).

To calculate the practical power resource of the northwest European shelf seas, and the spatial variability in the potential installed array capacity factor, we consider the extractable resource for an observed power curve from a grid-connected prototype turbine – the Seagen-S twin 600 kW (net 1.2 MW), 16 m diameter, turbine deployed in Strangford Narrows, UK (www.marineturbines.com). We simulate tidal currents in their present, natural state; i.e., power extraction from individual turbines has not been simulated. The practical power resource is calculated, post-simulation, by fitting a polynomial curve to the observed flood/ebb averaged power curve of the Seagen-S device, where the cut-in and rated power speeds are 1.0 and 2.7 m s^{-1}, respectively. Practical power has then been calculated based on depth-averaged simulated velocities and the power curve. Therefore, several impacts of power extraction have not been considered in our overall resource characterisation, such as the vertical current profile, turbine wake effects and blockage effects, turbine optimisation within an array, and array-array interactions between neighbouring sites.

4. Variability of the tidal energy resource

4.1. Peak tidal currents

Maximum depth-averaged tidal velocities across the northwest European shelf seas have been calculated at a horizontal resolution of approximately 1 km (Fig. 2). Here, we present the summation of the principal 5 tidal constituents derived from our tidal analysis (*see* Section 2); hence currents of this magnitude require all 5 of these constituents to be in-phase, and will occur less regularly than every lunar cycle – approximately once per year, in accordance with the solar annual (S_a) long period tide [34]. High energy sites suitable for 'first-generation' technologies require mean spring peak current speeds to exceed 2.5 m s^{-1} and water depths to be in the range 25–50 m [14], whereas 'second-generation' technologies have been defined as requiring mean spring peak current speeds to exceed 2 m s^{-1} and water depths to exceed 25 m [12]. Based on both first- and second-generation technologies, our analysis has isolated several suitable locations for the deployment of TEC arrays (regions within the black contours in Fig. 2). These potential TEC locations can be grouped into the following main regions: (1) Northern Scotland, particularly around Orkney, and Faroe; (2) The Irish Sea (noticeably The Bristol Channel, northwest Anglesey, and southwest Scotland); and (3) The English Channel (noticeably near Brittany, Normandy, and The Channel islands). These high-energy regions generally occur due to tidal streaming around headlands and islands, through channels, or in shallow waters, and cover a surface area of approximately 9500 km^2 (which is approximately 0.5% of the area of the northwest European shelf seas). Of particular note in Fig. 2 is the large potential sea space north of the Cherbourg Peninsula in the English Channel, which includes The Alderney Race, and is reported to have the capacity to deliver up to 7 TW h per annum of tidal energy (www.are.gg), which equates to approximately 2% of the energy generation of the UK [35].

In order to retain computational efficiency, our model resolution was not fine enough to fully resolve all potential sites at shelf scale; in particular, known high-velocity sites within the Orkney archipelago such as the Fall of Warness [13], or Ramsey Sound in southwest Wales [36]. Yet, for first-generation technologies, Lewis et al. [12] demonstrated that increasing model resolution beyond 1/60° does not drastically alter large-scale resource assessment. In order to characterise the extractable resource and/or optimise several aggregated, discrete development sites, it is desirable to understand the spatial variability in tidal currents, rather than simply their peak value, as is common in the majority of resource assessments (e.g., [1]).

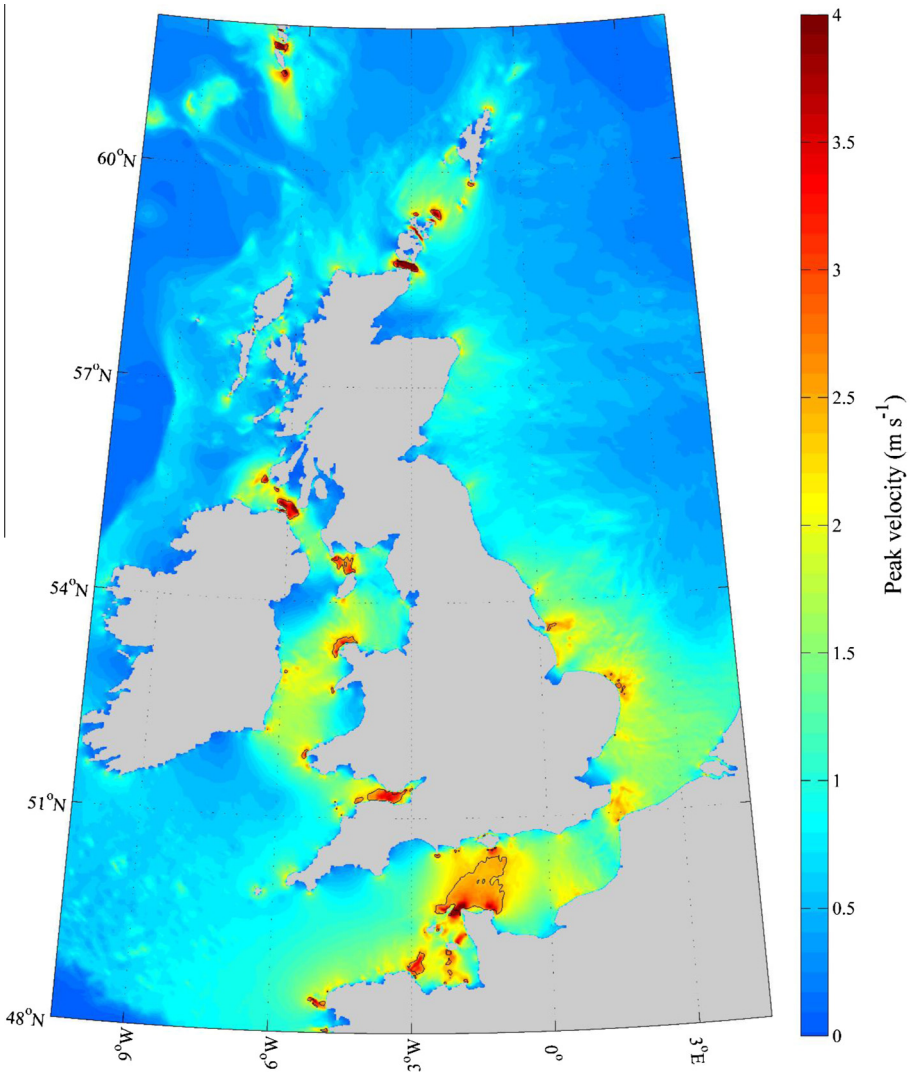

Fig. 2. Simulated maximum depth-averaged velocities within a sub-section of the northwest European shelf seas, based on tidal analyses of the following tidal constituents: M_2, S_2, K_1, O_1, and M_4. The black contours group all potential TEC sites – totalling 9500 km^2 where water depths exceed 25 m and mean spring peak velocities exceed 2 m s^{-1}.

4.2. Variability of tidal currents over lunar timescales

The spring-neap ratio R (Eq. (1)) has been calculated for the northwest European shelf seas (Fig. 3). The black contours in Fig. 3 correspond to those in Fig. 2, and denote potential first- and second-generation TEC sites – within which R varies from 0.59 (a relatively large variability between spring and neap flow) to 0.82 (a relatively low variability between spring and neap flow). Larger R ratios (coloured orange and red in Fig. 3) will generate a more continuous energy yield over the lunar cycle (i.e., minimising intermittency over semi-diurnal timescales) and, therefore, could be an important factor in resource exploitation and optimisation.

At potential TEC sites where there is a relatively large difference between the magnitudes of the spring and neap tidal current amplitudes, and consequently large variability in peak velocities over the spring-neap cycle, sub-optimal power will be generated during neap tides (where, for the majority of the time, currents do not attain the cut-in velocity threshold to generate power) and full power potential may not be realised during spring tides, due to the rated capacity of the turbine, as demonstrated in Fig. 4. In this example, we compare two contrasting sites with similar mean spring peak tidal velocities: a site off Alderney in the English Channel (Fig. 4a; $R = 0.75$) and a site in the Pentland Firth, Orkney (Fig. 4b; $R = 0.69$). In the Pentland Firth, significantly less practical power can be extracted (based on the Seagen-S turbine) for one week (during neaps) every fortnight, compared with the Alderney site (Fig. 4c and 4d), despite very similar mean spring peak tidal currents (3 m s^{-1}). When integrated over a year, the total annual power produced was 4.35 GW h at Alderney compared with 3.97 GW h in the Pentland Firth, based on the measured power curve for the grid-connected Seagen-S 1.2 MW rated turbine deployed in Strangford Narrows. This equates to a difference in annual power of approximately 387 MW h (i.e., approximately 10%), despite similar mean peak spring velocities. A similar pattern in the calculated theoretical power density is also shown (Fig. 4e and 4f).

When we examine all potential first- and second-generation TEC sites, for spring tidal flow, we show that more practical power can be extracted when R is greater (Fig. 5). In fact, we simulated that for locations where mean spring peak flow was approximately 3 m s^{-1}, the annual practical power generated from one device per model cell varied by approximately 750 MW h (i.e., approximately 15%), due to variations in the spring-neap ratio, R (Fig. 5). This difference equates to the annual energy usage for approximately 85 homes.[1]

[1] Assuming one home (in northwest Europe) uses energy at a rate of 1.0 kW h (World Energy Council: www.wec-indicators.enerdata.eu).

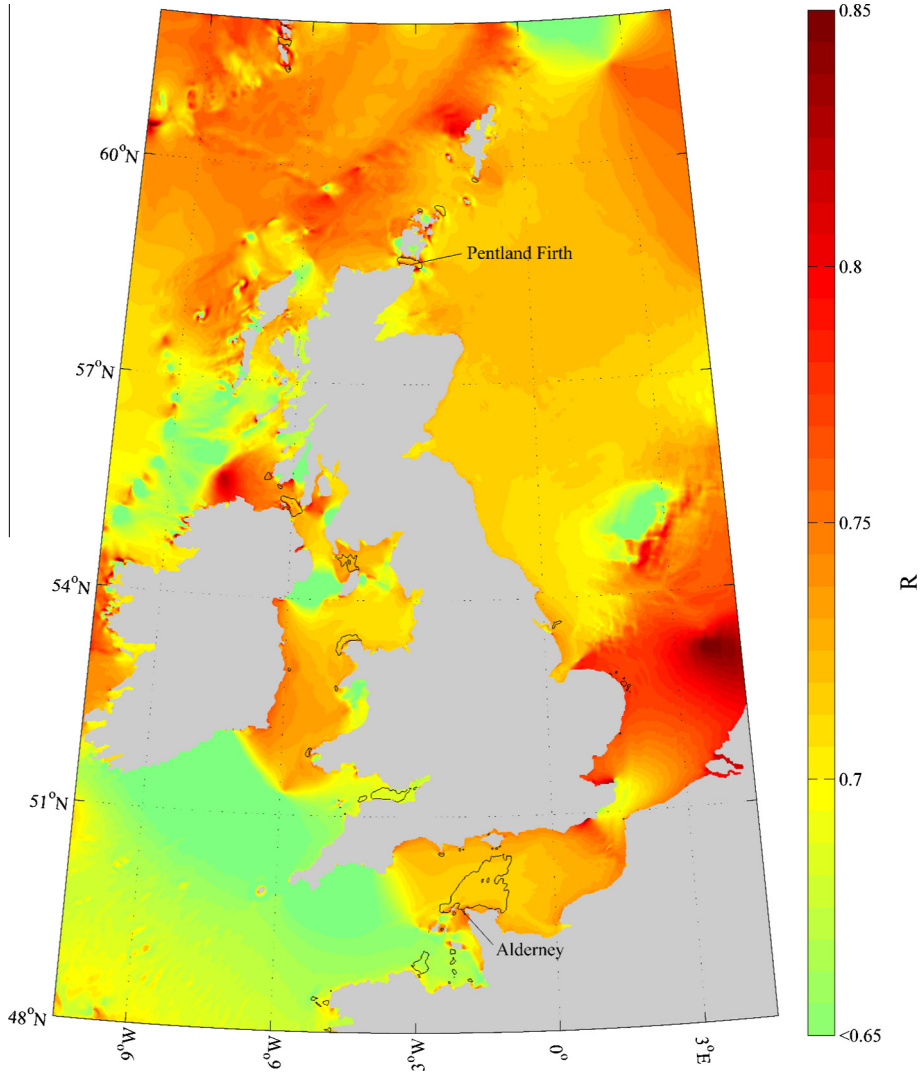

Fig. 3. Spatial variability in the simulated spring-neap cycle of tidal currents, plotted as a ratio R (Eq. (1)). The black contours group all potential TEC sites (*see* Fig. 2). Larger R ratios within the black contours signify a large M_2 velocity amplitude ($\overline{U}_{M2}$) relative to $\overline{U}_{S2}$, which will generate a more continuous energy yield over the lunar cycle than small R values. Values of $R < 0.65$ (outside potential TEC sites) have been set to 0.65 for better visualisation of potential TEC sites.

We present results based on one device per model cell. Assuming a device width of 45 m (i.e., the total width from the twin-rotor Seagen-S device; [37], lateral array spacing of 3 devices, and streamline array spacing of 10 devices [38], in a staggered formation [39], we estimate that the maximum capacity annual practical power can be up-scaled from the values above, by a factor of approximately 15, neglecting any device feedbacks. It is interesting to note that the higher tidal-stream sites all had values of R between 0.7 and 0.75. Further, it is also interesting to note that the 'tapering off' of power generation for higher peak velocities in Fig. 5 is due to excess power above rated velocities not being captured.

4.3. Diurnal variability of tidal currents

Simulated variability in the tidal current Form ratio, *Fu* (Eq. (2b)), has been calculated for the northwest European shelf seas (Fig. 6). Again, the black contours in Fig. 6 correspond to the potential first- and second-generation TEC sites shown in Fig. 2 – across which *Fu* varies by only a small amount, in the range 0.01–0.2, with a mean value of 0.03. However, we show that the variability in *Fu* does affect energy generation; there exists a relationship between *Fu* and generated power, for any given velocity (Fig. 7), based on the Seagen-S power curve. Indeed, higher values of *Fu* generally produce significantly less practical power, for any given velocity, than lower values of *Fu* (Fig. 7). For example, sites with maximum current speeds of 3 m s^{-1} produce annual practical power, deploying one device per model cell, in the range 2.5 GW h (high *Fu*) to 4.1 GW h (low *Fu*), which can be expressed as a ~40% change, depending on *Fu* (Fig. 7). Again, the above power values can be up-scaled by a factor of ~15 for maximum array sizes, neglecting device feedbacks.

4.4. Tidal asymmetry

Finally, the phase relationship between the principal semi-diurnal tidal current ($\emptyset_{\overline{U}M2}$) and its quarter-diurnal harmonic ($\emptyset_{\overline{U}M4}$) was calculated, according to Eq. (3). We present an example case where the flood and ebb currents are equal and the relative phase relationship is 90° (i.e., A = zero; Fig. 8a and 8b), and so, power generated on the flood and ebb phases of the tide is equal (Fig. 8d). Conversely, when the relative phase relationship is 0°, or 180°, and $A = \pm 1$, maximum asymmetry occurs; hence, stronger velocities are generated during the flooding tide than during the ebbing tide (Fig. 8a and 8c). Consequently, maximum power generation may occur once per tidal cycle, rather than twice, and the overall power production is reduced, compared with the symmetrical case,

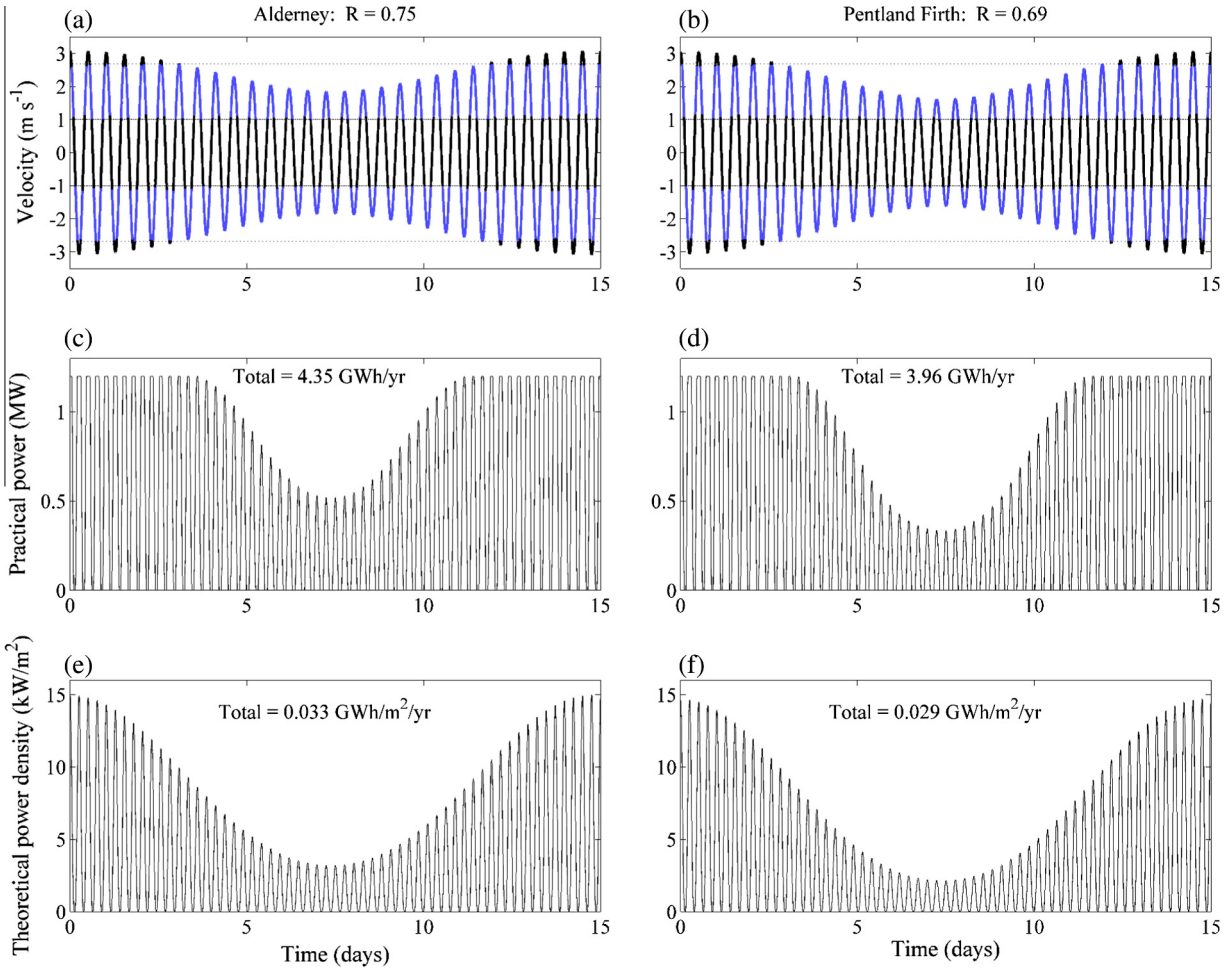

Fig. 4. Simulated depth-averaged tidal velocities ($\overline{U}_{M2} + \overline{U}_{S2}$)with spring-neap ratios (R, Eq. (1)) that are (a) large (Alderney, $R = 0.75$) and (b) small (Pentland Firth, $R = 0.69$). The blue curves indicate velocities which generate power, based on the measured Seagen-S power curve, and black curves indicate when velocities are either too small (below cut-in speeds) or exceed rated velocities and hence do not contribute to the 'practical power'. Panels (c) and (d) represent the corresponding practical power generated from (a) and (b), respectively, where total power output per year is also shown. Corresponding theoretical power density, and total power density per year, is plotted in panels (e) and (f), respectively.

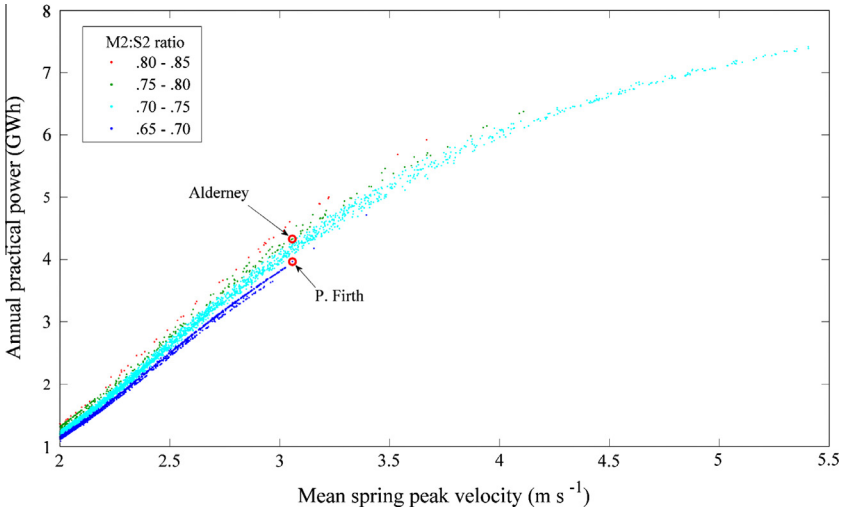

Fig. 5. Mean spring peak velocity plotted against annual practical power, for all potential TEC sites (*see* Fig. 2). Annual practical power values correspond to one device per model cell. Sites are coloured corresponding to their spring-neap ratio R (Eq. (1)), showing that, for any given peak flow, sites with a higher spring-neap ratio produce more practical power. Two contrasting sites (Alderney, $R = 0.75$, and Pentland Firth, $R = 0.69$), corresponding Fig. 4, are shown.

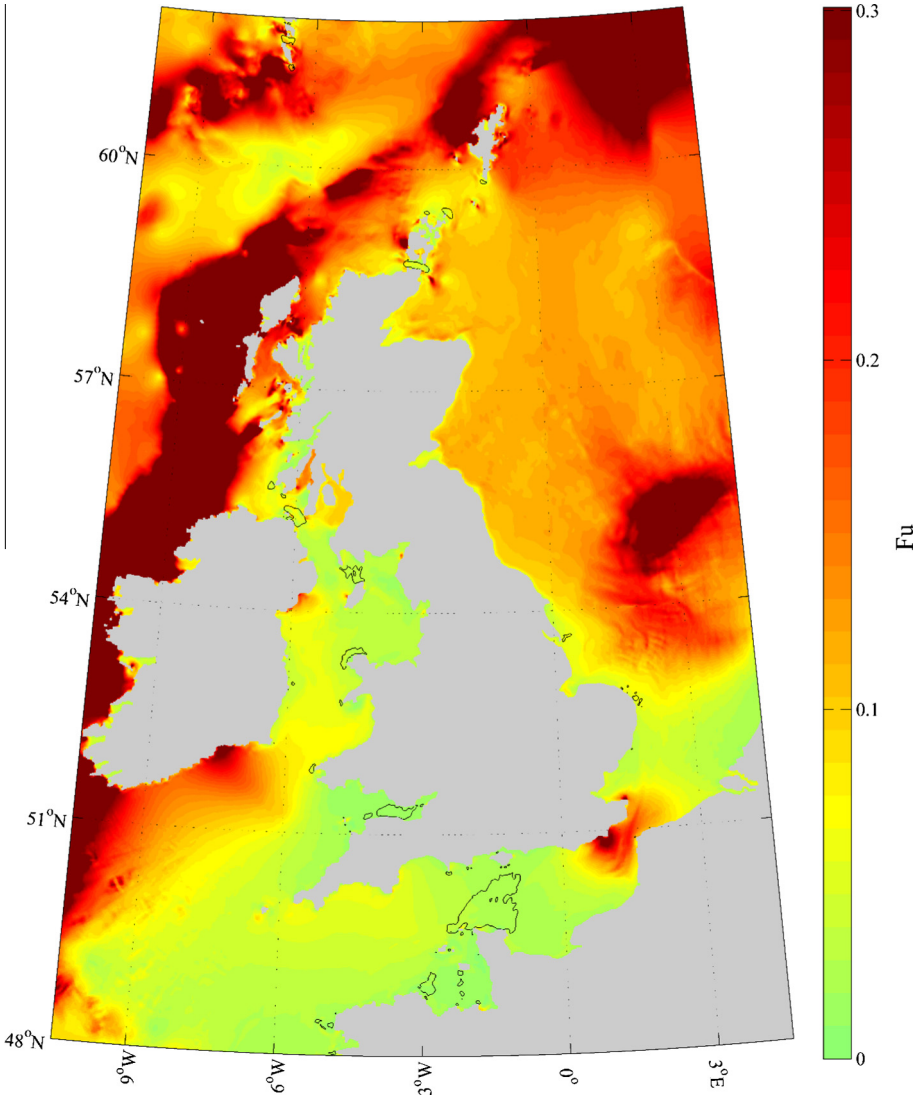

Fig. 6. Spatial variability in the tidal current Form ratio, *Fu* (Eq. (2a)). *Fu* has been capped at an upper bound of 0.3 in the figure in order to visualise variability between potential TEC sites – denoted by black contours as defined in Fig. 2.

even though peak velocity is higher (Fig. 8c and 8e). In our example (Fig. 8c), realistic tidal harmonics have been used at a site in the Pentland Firth, where we depicted strong tidal asymmetry and high values of ($\emptyset_{\overline{U}M4}$), relative to ($\emptyset_{\overline{U}M2}$) We compared the simulated ($\emptyset_{\overline{U}M4}$) with ($\emptyset_{\overline{U}M4} - 90^{\circ}$) (Fig. 8b). The relative phase shift of ($\emptyset_{\overline{U}M4}$) from tidal symmetry to asymmetry represents a reduction in power production of 55 MW h per year at this site, even though peak tidal velocities increase.

The simulated relative phase relationships between ($\emptyset_{\overline{U}M2}$) and ($\emptyset_{\overline{U}M4}$) (Eq. (3)) have been calculated and, so, provide a theoretical distribution of M_4-generated tidal asymmetry (Fig. 9a). Colours in the figure depict a normalised representation of symmetry/asymmetry, and our results, at least qualitatively, correspond well with theoretical simulations of M_4-generated net bed shear stress and sand transport pathways produced by Pingree and Griffith [20]. For example, we simulate tidal symmetry in the central Irish Sea (where bedload parting is known to occur; [40], tidal asymmetry around northwest Anglesey (an area which is attractive for TEC development, and where net sand transport is directed eastwards into Liverpool Bay; [6], and another region of symmetry, in the eastern Irish Sea (where sand accumulation takes place; [20] (Fig. 9a). In the English Channel, we simulate spatial gradients of tidal symmetry/asymmetry that mirror previous findings in the literature (e.g., [20,41,42]; at high energy locations in particular, such as around the Channel Islands, there is a complex distribution of tidal asymmetry (Fig. 9a), which may affect energy yield and lead to environmental issues associated with sediment transport [11,37,43].

Since the first harmonic of M_2 manifests itself in shallow coastal zones due to nonlinear frictional processes, the magnitude of the $\overline{U}_{M4}$ tidal currents are strongest in these regions. For our analysed potential TEC sites (i.e., 9500 km^2), $\overline{U}_{M4}$ tends to be relatively small (since we set a constraint on water depths greater than 25 m) – with a mean value of 0.094 m s^{-1} and standard deviation of 0.092 m s^{-1}. However, a maximum value for $\overline{U}_{M4}$ of 0.63 m s^{-1} was simulated, and approximately 10% of the sites experience $\overline{U}_{M4}$ greater than 0.2 m s^{-1}, indicating that the effects of the M_4 tide are important at these locations. Therefore, by calculating A' (Eq. (3)) spatially across the European shelf (Fig. 9a), and then multiplying A by the ratio $\overline{U}_{M4} : \overline{U}_{M2}$ (Fig. 9b), which we call A' (Eq. (4), Fig. 9c), we can determine the influence of M_4-generated tidal asymmetry to the energy yield:

$$A' = A * \frac{(\overline{U}_{M4})}{(\overline{U}_{M2})} \tag{4}$$

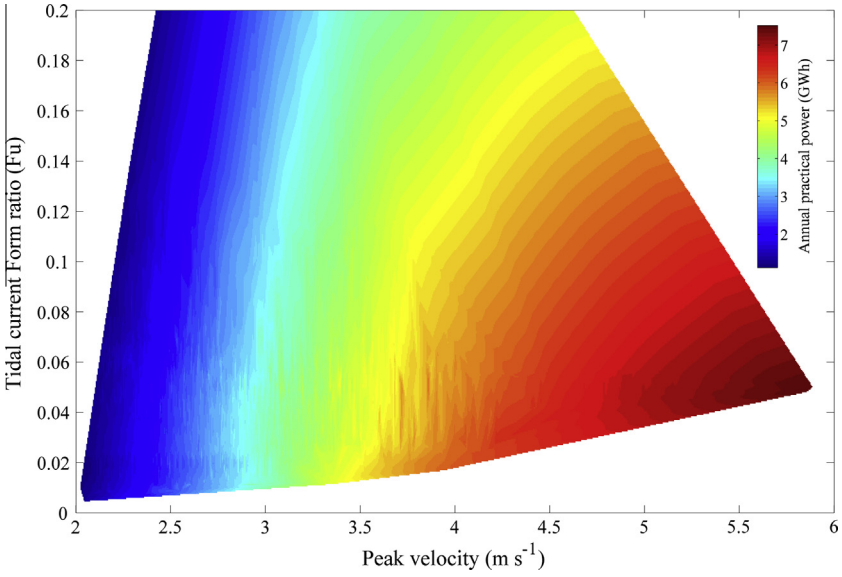

Fig. 7. Colour map of annual practical power, for potential TEC sites (i.e., 9500 km^2 where water depths exceed 25 m and velocities (M_2 + S_2) exceed 2 m s^{-1}), plotted relative to maximum depth-averaged velocity and the tidal current Form ratio, *Fu* (Eq. (2a)). Annual practical power values correspond to one device per model cell. (For interpretation of the references to colour in this figure legend, the reader is referred to the web version of this article.)

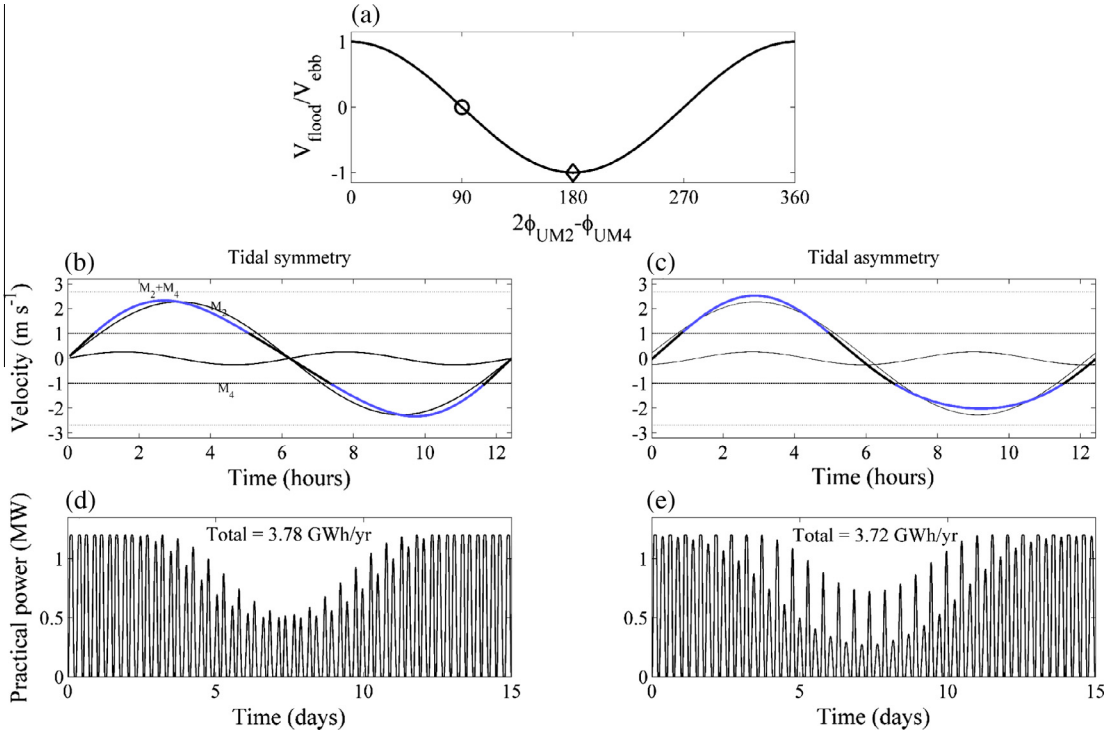

Fig. 8. (a) Theoretical tidal asymmetry, based on the relative phase relationships of $2\phi_{\overline{UM2}} - \phi_{\overline{UM4}}$ (degrees), plotted against normalised net tidal flow, where ±1 signifies maximum asymmetry and zero signifies symmetry. Two example tidal currents are shown; resulting in (b) tidal symmetry (i.e., $2\phi_{\overline{UM2}} - \phi_{\overline{UM4}} = 90°$; denoted by a circle in (a)) and (c) tidal asymmetry (i.e., $2\phi_{\overline{UM2}} - \phi_{\overline{UM4}} = 180°$; denoted by a diamond in (a)). M_2 and M_4 tidal velocities are shown (thin black curves), together with the resultant M_2 + M_4 (thick) curves (coloured blue above cut-in speeds, based on the Seagen-S power curve). Panels (d) and (e) represent the corresponding practical power generated from (b) and (c), respectively, over a spring-neap tidal cycle. Total power generation per year is also shown.

Further, at all potential TEC sites, we calculate the contribution of the M_4 tide to practical power, based on the Seagen-S power curve and assuming one device per model cell (Fig. 10). The contribution of M_4 tidal currents generally reduces power production, and there is a weak relationship based on tidal asymmetry; less net power production tends to occur when the tidal currents exhibit stronger asymmetry (Fig. 10).

4.5. Capacity factor

To summarise the variability in the tidal-stream energy resource, we have calculated the potential capacity factor across the northwest European shelf seas, which is perhaps a clearer characterisation/optimisation of the resource, albeit with less understanding of the physical processes provided in the previous

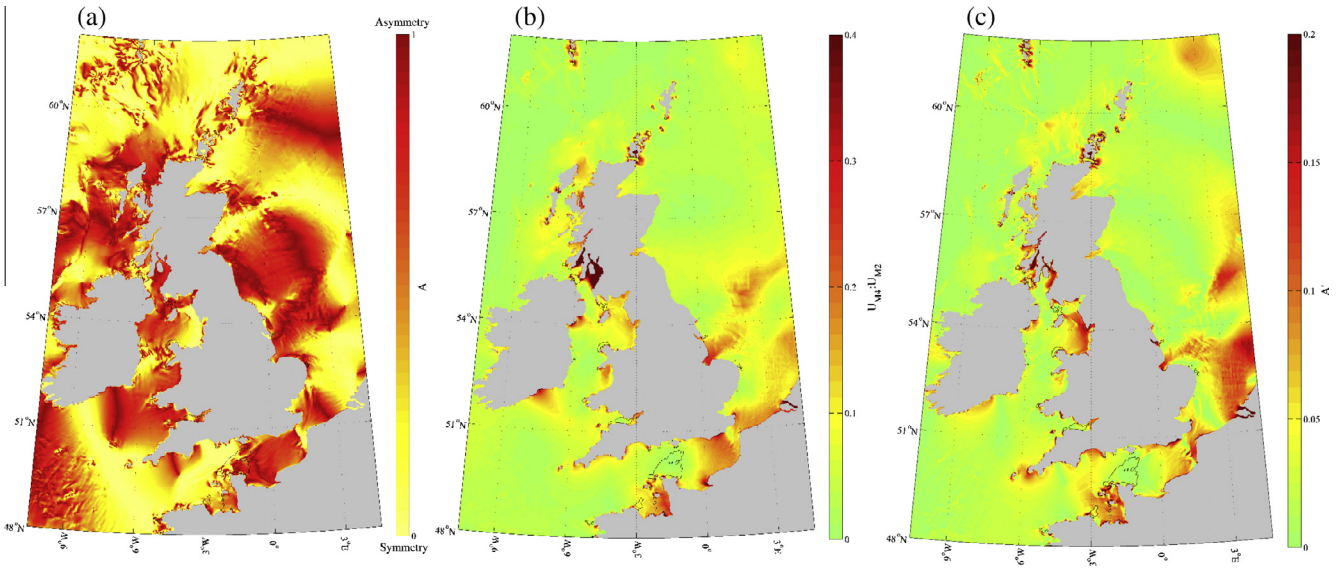

Fig. 9. Colour maps of (a) M_4-generated relative tidal asymmetry (A, Eq. (3)), (b) the ratio of tidal current amplitudes $\overline{U}_{M4} : \overline{U}_{M2}$., and (c) the tidal asymmetry metric A' (Eq. (4)). Red/orange areas in (a) show tidal asymmetry and yellow areas show tidal symmetry. The black contours denote potential TEC sites – where water depths exceed 25 m and mean spring peak velocities exceed 2 m s^{-1} (*see* Fig. 2) (For interpretation of the references to colour in this figure legend, the reader is referred to the web version of this article.)

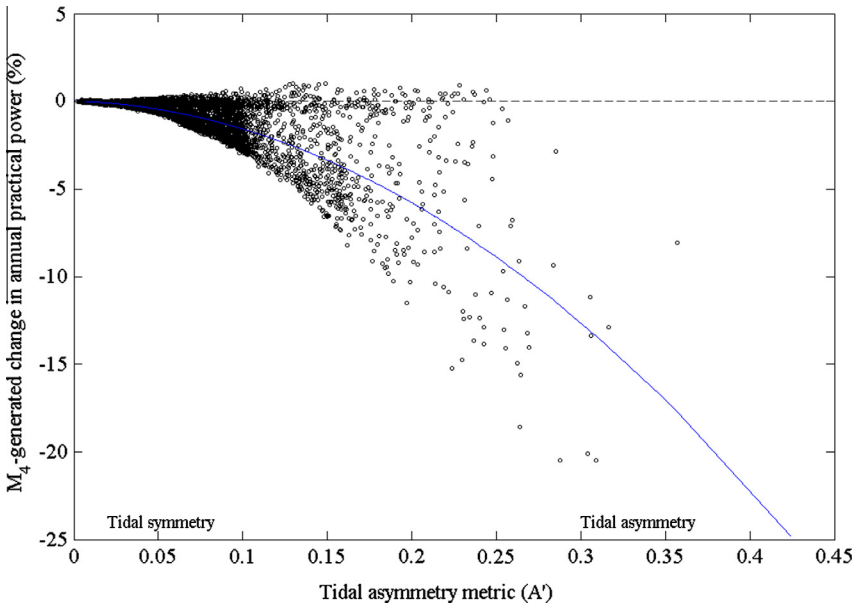

Fig. 10. A metric for tidal asymmetry (A', Eq. (4)), based on the relative phase relationships of $2\emptyset_{\overline{U}M2} - \emptyset_{\overline{U}M4}$ (Eq. (3)) and the ratio of tidal current amplitudes $\overline{U}_{M4} : \overline{U}_{M2}$, is plotted against M_4-generated change in practical power (i.e., the percentage difference between annual practical power generated from $[\overline{U}_{M2} + \overline{U}_{S2} + \overline{U}_{M4}]$ and $([\overline{U}_{M2} + \overline{U}_{S2}])$). Smaller values along the x-axis denote tidal symmetry, whereas larger values denote asymmetry. Negative values along the y-axis indicate M_4-generated reduction in power production, whereas positive values indicate increased power production. A quantile regression curve (solid blue) denotes the 50th quantile (i.e., line of best fit with polynomial order = 2) (For interpretation of the references to colour in this figure legend, the reader is referred to the web version of this article.)

analysis presented here. The capacity factor is defined here, following [21], as the mean power production over a year divided by the maximum (potential) power production. Explicitly, we calculate annual time series of power at each model grid cell over the northwest European shelf seas, based on the five analysed tidal constituents and the Seagen-S power curve. These time series capture power variability throughout different lunar cycles in a year, together with variability caused by diurnal inequalities and tidal asymmetries. The annual mean power production is then divided by the maximum produced power (usually the rated power value at potential TEC sites) to give the capacity factor at each model grid cell (Fig. 11). The capacity factor of most (96%) potential tidal-stream sites is below 50%, the average over the 9500 km^2 being 22%, although the maximum capacity factor calculated was approximately 70% in the Pentland Firth. As one might expect, higher velocity sites produce a larger capacity factor than lower tidal-stream sites, since current speeds reach rated capacity during a longer proportion of each tidal cycle.

5. Discussion

Semi-diurnal tides explain the majority of the tidal energy resource of the northwest European shelf seas [27]. Indeed, when

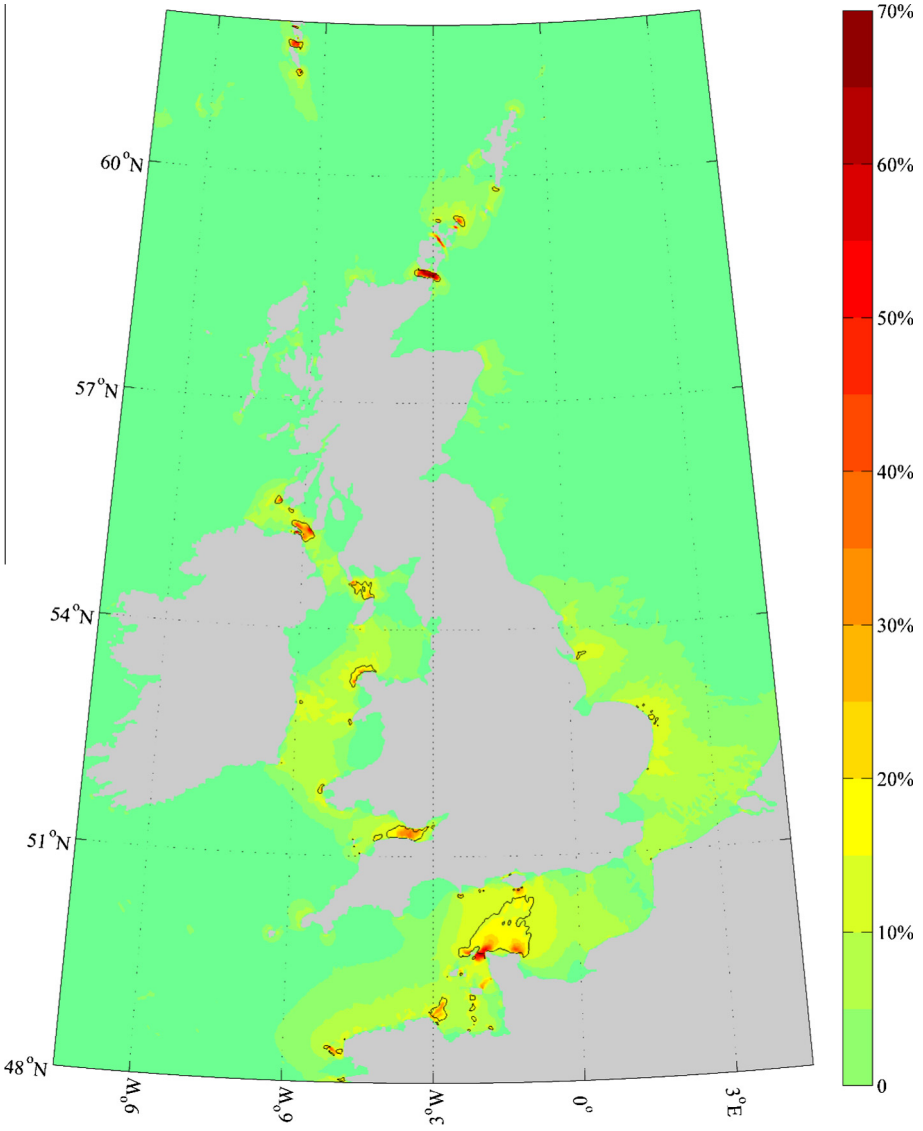

Fig. 11. Contour map of the annual Capacity factor of the northwest European shelf seas, based on the potential power production generated from the Seagen-S device. The primary five tidal constituents were considered in the calculations. The black contours denote all potential TEC sites (*see* Fig. 2).

we calculate the annual practical power at potential first- and second-generation TEC sites (i.e., 9500 km^2), produced by the 5 primary tidal constituents, the contribution from $M_2 + S_2$ accounts for 75%, or more, with an average contribution of 93%. The remaining 25%, or less, of annually generated power is produced by the remaining tidal constituents. At some sites, resource assessment based on the $M_2 + S_2$ constituents slightly over-predicts the total power production, by a few percent, due to the non-linear contributions when considering a wider range of constituents. For strongly semi-diurnal tidal environments, therefore, the first step in resource assessments should consider M_2 and S_2 tidal constituents, which we calculate contributes to an average of 93% of total practical power production. As a second step, more accurate resource assessments should consider lower current amplitude constituents such as, in the case of the northwest European shelf, K_1, O_1, and M_4.

We have demonstrated that there are large variabilities in the practical power produced at locations with similar 'mean spring peak velocities'. For example, applying the 1.2 MW Seagen-S device, we simulate annual variability in practical power generation of 15% for all sites with 3 m s^{-1} mean spring peak currents, due to variations in the spring-neap ratio, R (Eq. (1)); a large $\overline{U}_{S2}$ relative to $\overline{U}_{M2}$ generates less net power than a small $\overline{U}_{S2}$ relative to $\overline{U}_{M2}$. Indeed, mean spring peak velocities as low as 2.75 m s^{-1} with a high R ratio can produce as much power as 3 m s^{-1} sites with a low R ratio. Therefore, developers should consider spring-neap variability, as well as mean spring peak velocities. Potential sites with a small range in tidal currents, where $\overline{U}_{S2}$ is small relative to $\overline{U}_{M2}$, should be preferred for development. Also, these sites will produce a less intermittent electricity supply throughout the lunar cycle and could, therefore, be more attractive to developers.

Although the tides of the northwest European shelf are semi-diurnal, we have shown that additional tidal variabilities exist, which could be considered as operationally significant (i.e., up to 25% error) and, therefore, should be considered as a second step in resource assessments. Small diurnal inequalities stem from the tidal harmonics of K_1 and O_1, which range in combined tidal current amplitude from 0.02 to 0.42 m s^{-1}, at potential tidal-stream sites of the European shelf. In effect, when comparing several sites with similar peak tidal flows (such as from observational data), significant contributions from K_1 and O_1 tend to reduce the tidal

currents during one tide per day and, hence, reduce the practical power available when integrated over a year. Globally, tidal power density contributions from K_1 and O_1 tend to be largest (exceeding 1.5 MW m^{-2}) in the northeast Pacific [44], which is a region where tidal energy projects are being considered (e.g., in Cook Inlet, Alaska; en.openei.org).

Over a tidal cycle, we have found that more net power can potentially be generated if both the flood and ebb tidal currents are equal. At potential tidal-stream sites where relatively strong tidal asymmetries occur, usually in shallow water regions where the M_4 tide is relatively large and out-of-phase with M_2, we show that in most cases power production is reduced. Due to the challenges of electricity storage [45] and large variability in electricity demand and pricing throughout the day [46], significant daily and semi-diurnal variabilities in available power will render these sites less attractive for developers.

The criteria for first-generation tidal-stream energy development (water depths in the range 25–50 m and mean spring peak velocities greater than 2.5 m s^{-1}; [14] imposes a significant limitation of the resource in terms of available sea space [12]. For the northwest European shelf seas, this sea space equates to an areal extent of 850 km^2. If deeper waters were to be considered for development, and the velocity threshold reduced to 2 m s^{-1} (i.e., second-generation technologies), the exploitable sea space increases by an order of magnitude to 9500 km^2. Further, if the minimum water depth for deployment was reduced from 25 m to 20 m, the extractable surface area would increase by a further 7% and, importantly, these extra regions would be closer to shore, reducing cabling costs. However, to reduce blockage effects in shallow waters, the turbine cross sectional area, and so the power output, would need to be reduced [47]; hence, considerably less resource is contained in these shallower waters. Additionally, there are challenges faced by wave-current interactions in shallow waters [48].

In summary, for semi-diurnal tidal environments, we show that: (1) resource assessments should be based on power density rather than the mean spring peak velocities; (2) an operationally significant error (up to 25%) may occur if only M_2 and S_2 tidal constituents are considered; (3) the peak tidal velocity sites have less temporal variability from O_1, K_1, and M_4 tidal constituents; therefore, TEC devices with lower rated current speeds need to be developed to utilise the firm and predictable power generation potential within the European shelf seas (*see* [12]; and (4) there is high spatial variability of the capacity factor due to tidal constituents beyond the M_2 and S_2 signal, as shown in Fig. 11.

5.1. Assumptions and further research

Here we highlight several assumptions in our work – particularly in terms of calculating the practical resource, which, although largely beyond the scope of this study, should be the focus of future research in this important topic. Our results are based on realistic measurements of power efficiency from one particular horizontal-axis turbine design which has been deployed, optimised and grid-connected for one location in a tidal channel (Strangford Lough, UK). A different device and power curve applied to our modelled tidal velocities will lead to different results. Hence, a priority for the industry is to publish designed power curves for future tidal-stream energy sites/conditions. Therefore, we generalise practical power generation across the shelf, and it is important to note that more energy could potentially be generated by other turbines (e.g., [21] or by following site-specific turbine/array optimisation. However, many marine renewables companies are looking to develop 'off-the-shelf' technologies that can be installed at any location – similar to the situation in the present offshore wind industry – in which case our assumption is more appropriate.

For fixed-orientation, horizontal-axis turbines, the character of the tidal ellipse will affect the energy yield, and this has not been taken into account in our assessment of the resource. Peak flood and ebb tidal flows are assumed here to be fully exploitable by a turbine – in a way, assuming that the tidal currents are rectilinear and that turbines are orientated in-line with the tidal-stream to maximise power generation. In reality, many high-velocity regions are not rectilinear; for example, flood and ebb currents can be less than 180° out of phase due to bathymetric and topographic effects as the tide propagates around a headland or through a channel [12,21]. In such circumstances, fixed-orientation turbines cannot fully exploit both the flood and ebb tidal streams, so a degree of optimisation, or alternative (e.g., yawing) device design, is required. Although we apply a 3D model, we have not considered the vertical current profile in our calculation of the resource. Future studies may wish to assess the ability of models to simulate the vertical structure of the horizontal currents, and then re-calculate the resource within the operational depths of turbines.

Wave-tide interactions – the influence of waves on tidal currents – have not been simulated in this study, but have been shown to augment or reduce current speeds by up to 10% [10,11]. A projection of the tidal-stream resource, which also considers the stochastic nature of the climate, therefore, can be obtained in future studies by using coupled atmosphere-ocean-wave modelling systems, such as COAWST [10]. There are many other processes that will affect the practical power produced by a TEC array. For example, turbine optimisation within an array, and array-array interactions between neighbouring sites (e.g., adjacent model cells), have not been considered in this study. The impact of power extraction, wake effects and blockage effects, on the downstream flow and surrounding flow will affect the resource [49,50]. However, array configuration strategies are largely unknown and project-specific, and, if lower tidal velocity sites are developed, turbine interaction with the resource itself is not well understood/represented – especially at lower velocity and deeper water sites.

6. Conclusions

We have developed a high-resolution three-dimensional ocean model of the northwest European shelf seas – a region with some of the highest tidal dissipation in the world and surrounded by nations that are motivated to invest in marine renewables due to policy and wealth. We have calculated the European tidal-stream energy resource at higher resolution than has previously been achieved. We have shown that harmonic variabilities in the tidal currents can cause significant variabilities in the annual practical power that is available at potential tidal-stream energy sites. However, there tends to be less variability (~10%) between lower energy sites (e.g., sites with mean peak spring velocities around 2 m s^{-1}) than between higher energy sites (e.g., sites with mean peak spring velocities around 3 m s^{-1}). Hence, counter-intuitively, site selection based on lower rated turbines, where a larger sea space is available, may generate more electricity than higher rated turbines which can only be placed over a relatively limited sea space. Further, the instantaneous energy production from lower energy sites will be more evenly distributed throughout a lunar cycle, which could be regarded as lower risk to potential developers.

Traditional methods of calculating the tidal-stream energy resource based on the mean spring-neap tide may inaccurately represent the resource. Where other tidal constituents become significant in terms of current amplitude and/or phase, such as S_2, K_1, O_1 and M_4, it will be important for potential developers to resolve these constituents (i.e., velocity measurements should be of an appropriate duration for tidal analysis) in their calculation of the resource and relate the energy production to corresponding daily

and seasonal peaks in energy demand. Moreover, if firm power generation or phasing solutions are favoured within and across tidal energy developments, we find additional significant temporal variability within the high tidal current flows of the European shelf seas.

Acknowledgements

This work was undertaken as part of the following research projects: LCRI-M (Low Carbon Research Institute – Marine Consortium; www.lcri.org.uk, Grant Number 80284), SEACAMS (Sustainable Expansion of the Applied Coastal and Marine Sectors; www.seacams.ac.uk, Grant Number 80366), and EPSRC Supergen project EP/J010200/1. The authors acknowledge the financial support of the Welsh Government, the Higher Education Funding Council for Wales, the Welsh European Funding Office, and the European Regional Development Fund Convergence Programme. The extensive model simulations were achieved through access to High Performance Computing (HPC) Wales, a collaboration between Welsh universities, the Welsh Government, and Fujitsu.

References

[1] ABPmer. 2008. Atlas of UK Marine Renewable Energy Resources. 2008. ABPmer. Date of access (26 June 2014) <http://www.renewables-atlas.info/>.
[2] Ramos V, Carballo R, Álvarez M, Sánchez M, Iglesias G. A port towards energy self-sufficiency using tidal stream power. Energy 2014;71:432–44.
[3] Bryden IG, Couch SJ. ME1 marine energy extraction: tidal resource analysis. Renewable Energy 2006;31:133–9.
[4] Kadiri M, Ahmadian R, Bockelmann-Evans B, Rauen W, Falconer R. A review of the potential water quality impacts of tidal renewable energy systems. Renew Sustain Energy Rev 2012;16:329–41.
[5] Neill SP, Jordan JR, Couch SJ. Impact of tidal energy converter (TEC) arrays on the dynamics of headland sand banks. Renewable Energy 2012;37:387–97.
[6] Robins PE, Neill SP, Lewis MJ. Impact of tidal-stream arrays in relation to the natural variability of sedimentary processes. Renewable Energy 2014;72:311–21.
[7] Vazquez A, Iglesias G. Public perceptions and externalities in tidal stream energy: a valuation for policy-making. Ocean Coast Manag 2015;105:15–24.
[8] Egbert GD, Ray RD. Significant dissipation of tidal energy in the deep ocean inferred from satellite altimeter data. Nature 2000;405:775–8.
[9] Egbert GD, Ray RD. Semi-diurnal and diurnal tidal dissipation from Topex/Poseidon altimetry. Geophys Res Lett 2003;30:1907.
[10] Hashemi MR, Neill SP, Davies AG. A coupled tide-wave model for the NW European shelf seas. Geophys Astrophys Fluid Dyn 2014. http://dx.doi.org/10.1080/03091929.2014.944909.
[11] Lewis M, Neill S, Hashemi MR. Realistic wave conditions and their influence on quantifying the tidal-stream energy resource. Appl Energy 2014;136:495–508.
[12] Lewis MJ, Neill SP, Robins PE, Hashemi MR. Resource assessment for the next generation of tidal-stream arrays. Energy 2015. http://dx.doi.org/10.1016/j.energy.2015.02.038.
[13] Neill SP, Hashemi MR, Lewis MJ. The role of tidal asymmetry in characterizing the tidal energy resource of Orkney. Renewable Energy 2014;68:337–50.
[14] Iyer A, Couch S, Harrison G, Wallace A. Variability and phasing of tidal current energy around the United Kingdom. Renewable Energy 2013;51:343–57.
[15] Neill SP, Hashemi MR, Lewis MJ. Optimal phasing of the European tidal stream resource using the greedy algorithm with penalty function. Energy 2014;73:997–1006.
[16] Pugh DT. 1996. Tides, surges, and mean sea-level. John Wiley and Sons Ltd, Chichester. 2nd Edn., 1996, 472 pp.
[17] Simpson JH, Sharples J. The physical and biological oceanography of the shelf seas. Cambridge University Press; 2012. p. 424.
[18] Pingree RD, Griffith DK. S_2 tidal simulations on the northwest European shelf. J Mar Biol Assoc 1981;61:609–16.
[19] Pond S, Pickard GL. 1978. Introductory Dynamic Oceanography. Pergamon Press Ltd., Oxford. 2nd ed., 1978, 329 pp.
[20] Pingree RD, Griffith DK. Sand transport paths around the British Isles resulting from M2 and M4 tidal interactions. J Mar Biol Assoc UK 1979;59:497–513.
[21] Polagye B, Thomson J. Tidal energy resource characterization: methodology and field study in Admiralty Inlet, Puget Sound, WA (USA). Proc IMechE Part A: J Power Energy 2013;227:352–67.
[22] Shchepetkin AF, McWilliams JC. Regional Ocean Model System: a split-explicit ocean model with a free-surface and topography-following vertical coordinate. Ocean Model 2005;9:347–404.
[23] Shchepetkin AF, McWilliams JC. Correction and commentary for "ocean forecasting in terrain-following coordinates: formulation and skill assessment of the regional ocean modeling system" by Haidvogel et al. J Comp Phys 2009;227:3595–624 [J Comput Phys, vol. 228: p. 8985-9000].
[24] Egbert GD, Erofeeva SY. Efficient inverse modeling of barotropic ocean tides. J Atmos Oceanic Technol 2002;19:183–204.
[25] Warner JC, Sherwood CR, Arango HG, Signell RP. Performance of four turbulence closure methods implemented using a generic length scale method. Ocean Model 2005;8:81–113.
[26] Haidvogel DB, Arango H, Budgell WP, Cornuelle BD, Curchitser E, Di Lorenzo E, et al. Ocean forecasting in terrain-following coordinates: Formulation and skill assessment of the Regional Ocean Modeling System. J Comput Phys 2008;227:3595–624.
[27] Hashemi MR, Neill SP. The role of tides in shelf-scale simulations of the wave energy resource. Renewable Energy 2014;69:300–10.
[28] Pawlowicz R, Beardsley B, Lentz S. Classical tidal harmonic analysis including error estimates in MATLAB using T_TIDE. Comput Geosci 2002;28:929–37.
[29] Egbert GD, Erofeeva SY, Ray RD. Assimilation of altimetry data for nonlinear shallow-water tides: quarter-diurnal tides of the Northwest European Shelf. Cont Shelf Res 2010;30:668–79.
[30] Neill SP, Scourse JD, Uehara K. Evolution of bed shear stress distribution over the northwest European shelf seas during the last 12,000 years. Ocean Dynamics 2010;60:1139–56.
[31] Jones J. 1983. Charts of O1, K1, N2, M2 and S2 tides in the Celtic Sea including M2 and S2 tidal currents. Tech. rep.
[32] Davies AM, Jones JE. Application of a three-dimensional turbulence energy model to the determination of tidal currents on the northwest European Shelf. J Geophys Res 1990;95(C10):18143.
[33] Young EF, Aldridge JN, Brown J. Development and validation of a three-dimensional curvilinear model for the study of fluxes through the North Channel of the Irish Sea. Cont Shelf Res 2000;20:997–1035.
[34] Wunsch C. The long-period tides. Rev Geophys 1967;5:447–75.
[35] Strbac G, Shakoor A, Black M, Pudjianto D, Bopp T. Impact of wind generation on the operation and development of the UK electricity systems. Electric Power Syst Res 2007;77:1214–27.
[36] Fairley I, Evans P, Wooldridge C, Willis M, Masters I. Evaluation of tidal stream resource in a potential array area via direct measurements. Renewable Energy 2013;57:70–8.
[37] Neill SP, Scource JD. The formation of headland/island sandbanks. Cont Shelf Res 2009;29:2167–77.
[38] Myers LE, Bahaj AS. An experimental investigation simulating flow effects in first generation marine current energy converter arrays. Renewable Energy 2012;37:28–36.
[39] Couch SJ, Bryden IG. 2007. Large-scale physical response of the tidal system to energy extraction and its significance for informing environmental and ecological impact assessment. In: Proceedings Oceans 2007-Europe International Conference 2007, p. 912–6.
[40] Van Landeghem KJJ, Uehara K, Wheeler AJ, Mitchell NC, Scourse JD. Post-glacial sediment dynamics in the Irish Sea and sediment wave morphology: data-model comparisons. Cont Shelf Res 2009;29:1723–36.
[41] Pingree RD, Maddock L. Tidal residuals in the English Channel. J Mar Biol Assoc United Kingdom 1977;57:339–54.
[42] Grochowski NTL, Collins MB, Boxall SR, Salomon J-C, Breton M, Lafite R. Sediment transport pathways in the Eastern English Channel. Oceanol Acta 1993;16:531–8.
[43] Lewis MJ, Neill SP, Elliott AJ. Interannual variability of two offshore sand banks in a region of extreme tidal range. J Coastal Res 2014;31:265–75.
[44] Wang Y, Fang G, Wei Z, Wang Y, Wang X, Xu X. Cotidal charts and tidal power input atlases of the global ocean from TOPEX/Poseidon and JASON-1 altimetry. Acta Oceanologica Sinica 2012;31:11–23.
[45] Manchester S, Barzegar B, Swan L, Groulx D. Energy storage requirements for in-stream tidal generation on a limited capacity electricity grid. Energy 2013;61:283–90.
[46] Dupont B, De Jonghea C, Olmosb L, Belmansa R. Demand response with locational dynamic pricing to support the integration of renewables. Energy Policy 2014;67:344–54.
[47] Adcock TAA, Draper S, Houlsby GT, Borthwick AGL, Serhadlioglu S. The available power from tidal stream turbines in the Pentland Firth. Proc R Soc A 2013;469. http://dx.doi.org/10.1098/rspa.2013.0072.
[48] Hashemi MR, Neill SP, Robins PE, Davies AG, Lewis MJ. Effect of waves on the tidal energy resource at a planned tidal-stream array. Renewable Energy 2015;75:626–39.
[49] Malki R, Masters I, Williams AJ, Croft TN. Planning tidal stream turbine array layouts using a coupled blade element momentum - computational fluid dynamics model. Renewable Energy 2014;63:46–54.
[50] Consul CA, Willden RHJ, McIntosh SC. Blockage effects on the hydrodynamic performance of a marine cross-flow turbine. Philos Trans Royal Soc A-Math Phys Eng Sci 2013;371. http://dx.doi.org/10.1098/rsta.2012.0299.